IEEE Access
Multidisciplinary | Rapid Review | Open Access Journal

Received 17 November 2023, accepted 13 December 2023, date of publication 28 December 2023,
date of current version 9 January 2024.

Digital Object Identifier 10.1109/ACCESS.2023.3347919

RESEARCH ARTICLE

Computationally Efficient Blind Source Separation-Based MIMO-PA Linearization

SHIPRA, (Student Member, IEEE), AND MEENAKSHI RAWAT, (Member, IEEE)
Department of Electronics and Communication, Indian Institute of Technology Roorkee, Roorkee 247667, India

Corresponding author: Meenakshi Rawat (meenakshirawat@ieee.org)

This work was supported by the Research and Development Work carried out in the Project under 59/I4/02/2023-BRNS/39016 and Impacting Research Innovation and Technology-II (IMPRINT-II), India, under the Grant IMP/2018/001569.

ABSTRACT This paper presents a Cross-Interference Reduction Digital predistortion (CIR-DPD) for a multiple-input and multiple-output (MIMO) system. The proposed method cancels the detrimental effect of crosstalk due to different MIMO branches and the antenna reflection from the same antenna. This technique incorporates an Independent Component Analysis (ICA) algorithm-based source separation technique to find the mixing matrix developed due to crosstalk and antenna reflection. Further, this mixing matrix is used to predict the pre-cancellation of antenna reflection and crosstalk matrix. The proposed CIR-ICA model furnishes a two-step single-iteration digital mitigation solution to multiple branches of MIMO transmitters. Compared to current DPD techniques, the proposed CIR-DPD model enables suitable detection for transmitter defects while lowering its complexity. The experimental proof-of-concept for the 4×4 MIMO transmitter is presented in the presence of crosstalk, PA nonlinearity, and antenna reflection.

INDEX TERMS Crossover memory polynomial, digital predistortion (DPD), independent component analysis, multiple input multiple outputs, normalized mean square error.

I. INTRODUCTION

The Massive multiple-input and multiple-output (MIMO) technology has effectively demonstrated its vast potential for upgrading productivity in the fifth generation (5G) cellular networks [1]. The key thought is to furnish base stations with numerous, controllable antennas to provide multiple users over the same time-frequency resources through spatial multiplexing [2]. The base station should be designed utilizing low-complexity processing schemes and lower-cost equipment to make MIMO industrially feasible. Therefore, managing hardware imperfections is one of the principal obstacles in making Massive MIMO essentially attainable. Moreover, with the advancement of present-day wireless technologies, digital predistortion (DPD) [3] is extensively utilized to remove the nonlinear distortions generated by the transmitters/RF power amplifiers (PAs) [4], [5]. DPD is a popular solution to deliver better linearization performance with lower complexity in several applications [6], [7].

The Volterra-Series-based DPD models and their variants, such as memory polynomial (MP) and generalized MP, were reported in [3], [4], and [5] for the PA linearization in Single-Input-single-output transmitter. The MIMO transmitters' crossover MP model (COMP) [8] assumes linear cross-interference between the MIMO branches. Parallel Hammerstein (PH) model [9] compensates for nonlinear crosstalk and PA nonlinearity, making it more effective but more complex than the COMP Model. Reference [10] presented a DPD model based on a neural network for addressing DC offset, crosstalk, PA nonlinearity, and I/Q imbalance in MIMO transmitters. The limitations of these models are that these models become computationally inefficient and cumbersome due to a high number of coefficients when we increase the number of MIMO channels [11].

The associate editor coordinating the review of this manuscript and approving it for publication was Jagadheswaran Rajendran.

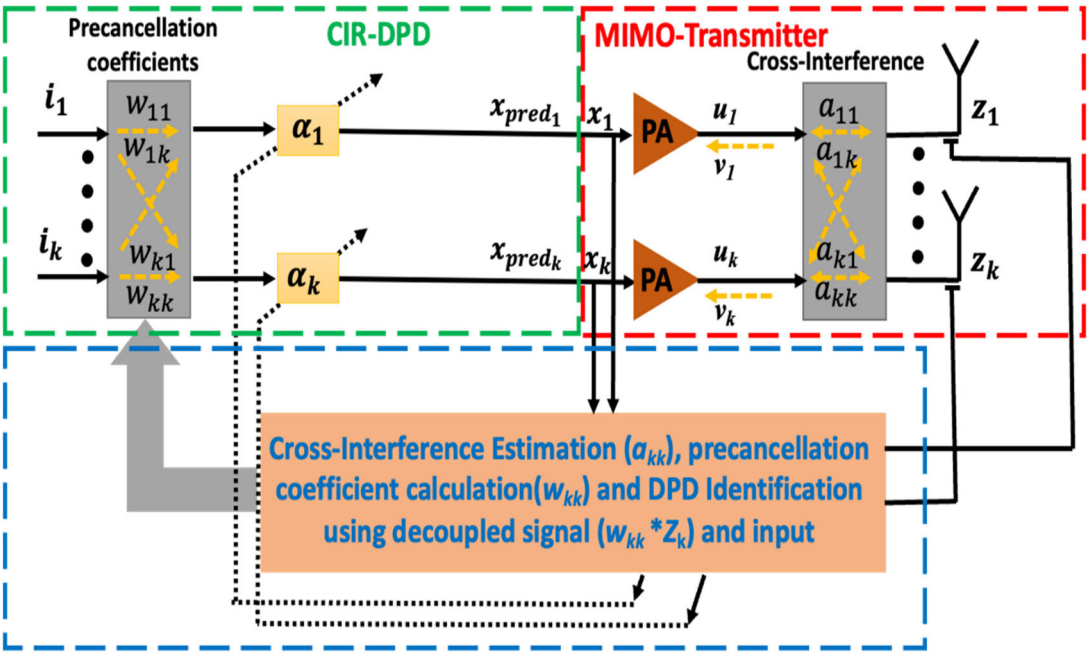

FIGURE 1. Block diagram of cross-interference reduction digital predistortion (CIR-DPD).

Recently, a dual-input DPD model was proposed in [12], where the dual-input PA model is paired with the linear antenna array model to combat the nonlinear crosstalk. This method is attractive as lesser coefficients are required leading to lower computational costs. However, the algorithm requires nonlinear optimization, where convergence relies on initial conditions, making it iterative, time-consuming, and challenging for practical implementation.

This paper presents the Cross-interference reduction Digital Predistortion (CIR-DPD) model, compensating for Power amplifier nonlinearity, crosstalk, and antenna reflection with lower computational cost. This method utilizes the concept of Blind signal separation (BSS) to characterize the cross-interference or crosstalk signal. BSS is a technique for retrieving a set of original signals from a group of mixed signals without knowing the source signals or the mixing mechanism [13]. When different source signal components are independent, then the process of separation of signals is called independent component analysis (ICA). When the intermixing of many separate signals causes distortions, the ICA approach is applied [14], [15], which has been used in wireless communications, radar, sonar, image, voice, and medical applications. The proposed CIR-DPD method utilizes the characteristics of ICA to generate the coefficients for pre-cancellation of antenna reflection and cross-interference along with DPD.

The paper is organized as follows. The system-level description of the DPD technique using ICA for cross-interference cancellation is given in Section II. Section III provides the algorithm for the proposed method and the established DPD models. Section IV describes the measurement setup for PA characterization and signals under test. Section V compares the performance of the proposed work with the state-of-the-art models. The results are provided in Section VI, followed by the conclusion.

II. SYSTEM MODEL

MIMO is a technology that can increase capacity along with radiated energy efficiency. An increase in capacity results from spatial multiplexing, and energy efficiency increases because of diversity using multiple antennas [1]. Implementing MIMO technology has become more strenuous as the number of antennas is increasing. The main challenge is cross-interference between the antenna arrays. This occurs because all the transmitted signals from the antennas couple with each other as they are on the same chip. Another major implementation challenge arises as a result of the nonlinear nature of the PA, which in turn, creates distortions in the transmitted signal.

Fig. 1 shows the system model of the MIMO transmitter, having k transmit paths. Every transmit path has a RF-PA, which is connected to the elements of the antenna array. Since it is a MIMO system, hence all the transmit paths operate at the same operating frequency. Fig.1 shows that i_k is the input in the baseband, and y_k is the output for the PA of the k_{th} path. This work adopts a two-step process: determining interference matrix A for each branch and calculating pre-cancellation coefficient w, using the ICA technique. Then, removing power amplifier nonlinearity using any established digital predistortion method. The system description is divided into two parts for better understanding: the proposed Cross-interference Reduction

(CIR) Model and the inverse modeling process for digital predistortion of the MIMO system. The composite digital predistortion model, which includes CIR and DPD, provides generalization for a high number of MIMO branches with much lower complexity.

The CIR DPD method, designed for $k \times k$ MIMO systems, entails a structured process. It begins with generating a baseband signal, $i(n)$=$[i_1(n)\ldots\ldots\ldots\ i_k(n)]$ followed by conversion into bandpass signals, $x(n)$ =$[x_1(n)\ldots\ldots\ldots x_k(n)]$ for transmission. These signals traverse power amplifiers known for introducing nonlinearity, crosstalk, and potential antenna reflections. After demodulation into the baseband domain, the output signals, $\mathbf{Z}$=$[z_1(n)\ldots\ldots z_k(n)]$ undergo essential cross-interference coefficient estimation, facilitated by ICA-based BSS method. Separated signals lead to the extraction of individual DPD coefficients for each MIMO branch. Precancellation coefficients derived during this process act as an un-mixing matrix, contributing to cross-interference mitigation. This matrix is applied to the input signal data, eventually generating predistorted signals. The final stage involves transmitting these predistorted signals through the MIMO transmitter to attain a linearized output. In essence, the CIR DPD method significantly improves MIMO system performance while upholding numerical stability and computational efficiency.

III. PROPOSED CIR-DPD MODEL

A. CROSS-INTERFERENCE REDUCTION (CIR) MODEL

The cross-interference between the branches and nonlinearity in the transmitter is a complex problem for the conventional DPD model.

The CIR Model models the cross-interference signals. The forward path signals $\mathbf{U}$ represent the output of power amplifiers (PAs). It can also be written as $\mathbf{U} = \mathrm{PA}\{x(n)\}$. The backward path signals $\mathbf{V}$ arise due to antenna reflection and are incident at the output of the same power amplifiers but in the opposite direction. These backward path signals are a consequence of the energy that is not radiated away from the antenna but rather reflected into the system.

$$\mathbf{U} = [\boldsymbol{u}_1 \ldots\ldots\ldots\ldots \boldsymbol{u_k}]^T \quad \text{forward path signals} \tag{1}$$

$$\mathbf{V} = [\boldsymbol{v}_1 \ldots\ldots\ldots\ldots \boldsymbol{v_k}]^T \quad \text{backward path signals} \tag{2}$$

It is observed that the backward path signals $\mathbf{V}$ are functions of the forward path signals $\mathbf{U}$, which establishes a causal relationship between them. Mathematically, this relationship is encapsulated by S-Parameters, which serve as coefficients that map the influence of forward path signals onto the backward path signals. S is the S-parameter matrix which can be expressed as:

$$\mathbf{S} = \begin{bmatrix} \boldsymbol{s}_{11} & \ldots\ldots\ldots & \boldsymbol{s}_{1k} \\ \cdot & & \cdot \\ \cdot & \ldots\ldots\ldots & \cdot \\ \cdot & & \cdot \\ \boldsymbol{s}_{k1} & \ldots\ldots\ldots & \boldsymbol{s}_{kk} \end{bmatrix} \tag{3}$$

The relation between the forward path signals and the backward path signals can be written as follows:

$$[\mathbf{v}_1 \ldots\ldots\ldots\ldots \mathbf{v}_k]^T = \begin{bmatrix} \boldsymbol{s}_{11} & \ldots\ldots\ldots & \boldsymbol{s}_{1k} \\ \cdot & & \cdot \\ \cdot & \ldots\ldots\ldots & \cdot \\ \cdot & & \cdot \\ \boldsymbol{s}_{k1} & \ldots\ldots\ldots & \boldsymbol{s}_{kk} \end{bmatrix} [\boldsymbol{u}_1 \ldots\ldots\ldots\ldots \boldsymbol{u}_k]^T \tag{4}$$

It can also be written as $\mathbf{V} = \mathbf{SU}$.

The signal $\mathbf{Z}$ combines forward and backward path signals when there is no cross-interference. It can be written as:

$$\mathbf{Z} = \mathbf{U} + \mathbf{V} \tag{5}$$

$$\mathbf{Z} = \mathbf{U} + \mathbf{SU} \tag{6}$$

$$\mathbf{Z} = (1 + \mathbf{S})\,\mathbf{U} \tag{7}$$

$$\boldsymbol{A} = 1 + \mathbf{S} \tag{8}$$

where $\boldsymbol{A}$ is called a mixing matrix and can be written as

$$\boldsymbol{A} = \begin{bmatrix} \boldsymbol{a}_{11} & \ldots\ldots & \boldsymbol{a_{1k}} \\ \cdot & \ldots\ldots\ldots & \cdot \\ \cdot & \ldots\ldots\ldots & \cdot \\ \boldsymbol{a_{k1}} & \ldots\ldots & \boldsymbol{a_{kk}} \end{bmatrix} \tag{9}$$

The z_k is the linear combination of the PA output of all transmit paths after cross-interference [12].

$$z_k = a_{k1}u_1 + a_{k2}u_2 + a_{k3}u_3 + \ldots + a_{kk}u_k \tag{10}$$

However, when the reflected signal has high power i.e. the power level which falls in the saturation region of power amplifier, it may impact the loading conditions of PA, and this reflected signal may intermingle with the incident signal. This will give rise to nonlinear terms such as $f(i_{\mathrm{k}}, v_{\mathrm{k}),}$ where f represents PA nonlinearity. In such cases,

$$z_k = f(x_k, a_{k1}u_1 + a_{k2}u_2 + a_{k3}u_3 + \ldots + a_{kk}u_k) \tag{11}$$

$\mathbf{Z} = [z_1, \ldots\ldots\ldots, z_k]^T$ denotes the matrix containing the observed baseband signal, measured at the output of the transmitter of the MIMO system having nonlinear cross-interference due to reflection from the antenna and PA nonlinearity. In the case of (8), the MIMO model can be mapped by the COMP model [8], which is a simplified case. In the case of (9), the PH model better describes the MIMO model [9], which provides a complete description of nonlinear cross-talk in MIMO transmission. The COMP model can be considered a simplified subset of the PH model, where only linear cross-talk is considered.

At lower power levels i.e., the power level used to describe conditions where the reflected power remains within the linear range of the power amplifier, the mixing matrix maintains linear relations, which allows the identification of the contribution of other signals on the k^{th} signal. The unmixing matrix enables inversion of the mixing matrix, which, when processed through the DPD block, allows predistortion of PA nonlinearity and the mixing matrix.

The ICA model is a generative model that defines how the components are mixed to produce the observed data. The mixing matrix is unknown. Based on the matrix **z**, the pre-cancellation coefficients using the ICA technique are calculated at the transmitter's output. The ICA technique can be applied using the FastICA algorithm. When compared to conventional ICA approaches, the FastICA algorithm and the contrast functions have several desirable qualities, such as:

1. The convergence is cubic in FastICA, whereas the ordinary ICA algorithms are based on (stochastic) gradient descent methods with linear convergence. This implies a rapid convergence.
2. Unlike gradient-based algorithms, there are no step size parameters to choose from. This indicates that the algorithm is simple to implement.
3. selecting a suitable nonlinear function, G can improve the method's performance. It is possible to obtain algorithms that are robust and/or have a low variance.
4. The independent components can be estimated one by one, similar to projection pursuit. This is important for exploratory data analysis as it reduces the method's computing overhead.
5. Most of the benefits of neural algorithms are available with the FastICA: It is distributed, parallel, computationally easy, and uses a small amount of memory. The stochastic gradient approach is superior only if quick adaptation in a changing environment is needed.

The Fast ICA Algorithm [16] is applied by first centering the observed signal matrix. It is done by subtracting its mean vector from the observed signal matrix.

$$\mathbf{Z} = \mathbf{Z} - E\{\mathbf{Z}\} \tag{12}$$

After centering the observation matrix, the mixing matrix is computed. The following preprocessing step is applied to whiten the matrix that, makes matrix A orthogonal.

$$\boldsymbol{A} = \mathbf{Q}\Lambda^{-1/2}\mathbf{Q}^H\mathbf{Z} \tag{13}$$

$$\text{where } \mathbf{Q}\Lambda\mathbf{Q}^H = E\left\{\mathbf{Z}\mathbf{Z}^H\right\} \tag{14}$$

$\mathbf{Q}$ is the matrix of eigenvectors, and Λ is the diagonal matrix of eigenvalues of $\boldsymbol{A}$. The inverse of $\boldsymbol{A}$ ($w = A^{-1}$) is computed after finding the mixing matrix $\boldsymbol{A}$, called the independent component matrix or the pre-cancellation coefficients.

The initial w can be taken as the arbitrary orthogonal matrix. The FastICA algorithm is an iterative method for locating a cost function's local maxima.

$$J_G = \sum_{i=1}^{k} E\left\{G\left(w_i^T\mathbf{Z}\right)\right\} \tag{15}$$

where i represent the rows of w_i, $i = 1,2,3\ldots k$, and G define the nonlinear function. The fourth-order cumulant, often known as kurtosis, is given below.

$$kurt(J_G) = E\left\{J_G^4\right\} - 3\left(E\left\{J_G^2\right\}\right)^2 \tag{16}$$

$w_i^T\mathbf{Z}$ should only have unit variance because $\mathbf{Z}$ is a unit.

Covariance matrix. In maximization of (16), the second term can be eliminated, and the cost function becomes

$$J_G^{kurt} = \sum_{i=1}^{k} E\left\{G\left(w_i^T\mathbf{Z}\right)^4\right\} \tag{17}$$

The independent component matrix is updated as

$$w^+ \leftarrow E\left\{\mathbf{Z}g\left(w^T\mathbf{Z}\right)\right\} - E\left\{g'\left(w^T\mathbf{Z}\right)\right\}w \tag{18}$$

where g is a derivate of G, called a contrast function and g' is the derivate of g. The first term of (16) is a gradient of J_G with respect to w_i, and the second term is because of Newton's approximation. The kurtosis contrast function is selected on the basis of two factors: the contrast function should be quick to compute, and the order in which the components are estimated [17]. Based on our cost function in (17), $g(x) = x^3$. The selection of the kurtosis contrast function as a cubic polynomial is desirable because polynomial functions are faster to compute than hyperbolic functions. Normalize the weights of matrix w after updating to improve stability. This is done as the weights lose their orthonormality on adaptation. The adaptation step (18), followed by normalization, is repeated until w converges.

$$w \leftarrow w^+ / \|w\| \tag{19}$$

w is defined as

$$w = \begin{bmatrix} w_{11} & \ldots & w_{1k} \\ \cdot & & \cdot \\ \cdot & \ldots & \cdot \\ \cdot & & \cdot \\ w_{k1} & \ldots & w_{kk} \end{bmatrix} \tag{20}$$

w_{ij} is the $k \times k$ matrix of the complex coefficients extracted from the ICA. k is the number of transmitters and receivers, respectively. The complexity comparison of different models is made such that the NMSE of the proposed model is equivalent to COMP's and PH's performance.

For the analysis of the BSS technique based on ICA separately from DPD, a simulation environment has been created where two signals interfere with each other in a noisy system. The results obtained by applying ICA show that the BSS technique based on ICA can significantly remove these interferences from the signal. The time-domain plots of the original interfered & noisy and cleaned signal using ICA are shown in Fig. 2, which depicts that the signal is cleaned significantly.

B. ESTABLISHED DPD MODELS

The linearization process can be performed using the direct or indirect learning method. The PA's output is used as the input for the pre-distorter block, which processes an inverse model of the PA in an indirect learning architecture (ILA) based DPD [18]. The block diagram of DPD using ILA is shown in Fig. 3. The input signal $x(n)$ is predistorted by the DPD block, which is denoted as $u(n)$ and sent through the PA. $y(n)$ is the output of PA, representing the post-processed version

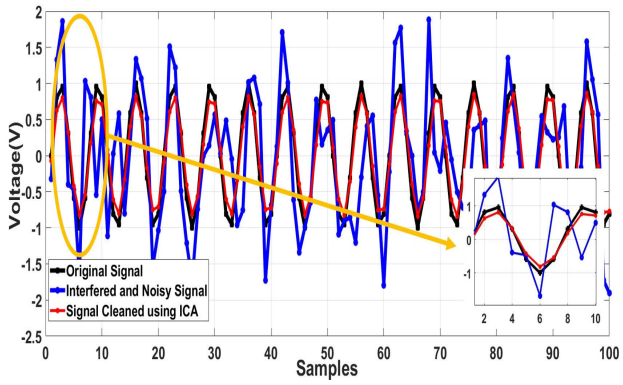

FIGURE 2. Time-domain plot of original signal, Interfered & noisy signal, and the signal after performing ICA.

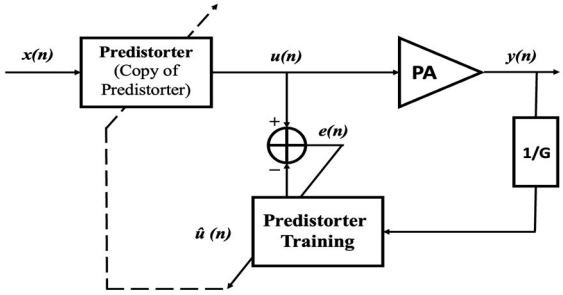

FIGURE 3. Block diagram of DPD using indirect learning architecture.

obtained from impairments cancellation. The coefficients are generated in the DPD block by inverse modeling of $y(n)$. Thereafter, the predistorted signal is created by multiplying the coefficients with the input signal.

This work shows the superiority of the proposed technique for memory polynomial basis function-based models. However, the proposed technique can be applied along with the digital mode having other basis functions. The popular DPD models with polynomial basis functions mentioned in the literature are as follows:

1) CROSSOVER MEMORY POLYNOMIAL (COMP) MODEL

The outcome of the Crossover *Memory Polynomial Model* [8] for 4 × 4 MIMO is given below:

$$\begin{aligned} y_{1COMPM}(n) = &\sum_{k=0}^{M}\sum_{q=0}^{Q-1}\alpha_{q,k}^{(1)}x_1(n-k)\,|x_1(n-k)|^q \\ &+\sum_{k=0}^{M}\sum_{q=0}^{Q-1}\beta_{q,k}^{(1)}x_2(n-k)\,|x_2(n-k)|^q \\ &+\sum_{k=0}^{M}\sum_{q=0}^{Q-1}\gamma_{q,k}^{(1)}x_3(n-k)\,|x_3(n-k)|^q \\ &+\sum_{k=0}^{M}\sum_{q=0}^{Q-1}\delta_{q,k}^{(1)}x_4(n-k)\,|x_4(n-k)|^q \end{aligned} \quad (21)$$

where x_1, x_2, x_3, and x_4 are separate baseband signals transmitted via distinct transmitters. The model coefficients are $\alpha_{q,k}$, $\beta_{q,k}$, $\gamma_{q,k}$ and $\delta_{q,k}$. The memory depth is denoted by M. The nonlinearity order of the above model is Q. In Crossover Memory Polynomial Model, the output of every transmitter consists of the component of all the other transmitters to consider the crosstalk effect.

2) MEMORY POLYNOMIAL (MP) MODEL

(22) gives the output of the MP model [12] for each individual transmitter.

$$y_{MPM}(n) = \sum_{k=0}^{M}\sum_{q=0}^{Q-1}\alpha_{q,k}x(n-k)\,|x(n-k)|^q \quad (22)$$

where Q is the nonlinearity order, and M denotes the memory depth of the MP Model. The MP model does not consider compensation for the nonlinear cross-interference term.

However, it is a popular model to compensate for the PA nonlinearity.

3) PARALLEL HAMMERSTEIN MODEL

The Parallel Hammerstein model's output [9] given for 4 × 4 MIMO is shown in (23).

$$\begin{aligned} &y_{1PHM}(n) \\ &== \sum_{k=0}^{M}\sum_{q=0}^{Q-1}\sum_{j=0}^{q}\sum_{i=0}^{j}\sum_{k=0}^{i}\alpha_{q,j,i,l}^{(1)}x_1(n-k)\,|x_1(n-k)|^{q-j} \\ &\cdot|x_2(n-k)|^{j-i}\,|x_3(n-k)|^{i-l}\,|x_4(n-k)|^{l} \\ &+\sum_{k=0}^{M}\sum_{q=0}^{Q-1}\sum_{j=0}^{q}\sum_{i=0}^{j}\sum_{l=0}^{i}\beta_{q,j,i,l}^{(1)}x_2(n-k)\,|x_1(n-k)|^{q-j} \\ &\cdot|x_2(n-k)|^{j-i}\,|x_3(n-k)|^{i-l}\,|x_4(n-k)|^{l} \\ &+\sum_{k=0}^{M}\sum_{q=0}^{Q-1}\sum_{j=0}^{q}\sum_{i=0}^{j}\sum_{l=0}^{i}\gamma_{q,j,i,l}^{(1)}x_3(n-k)\,|x_1(n-k)|^{q-j} \\ &\cdot|x_2(n-k)|^{j-i}\,|x_3(n-k)|^{i-l}\,|x_4(n-k)|^{l} \\ &+\sum_{k=0}^{M}\sum_{q=0}^{Q-1}\sum_{j=0}^{q}\sum_{i=0}^{j}\sum_{l=0}^{i}\delta_{q,j,i,l}^{(1)}x_4(n-k)\,|x_1(n-k)|^{q-j} \\ &\cdot|x_2(n-k)|^{j-i}\,|x_3(n-k)|^{i-l}\,|x_4(n-k)|^{l} \end{aligned} \quad (23)$$

where, the Parallel Hammerstein (PH) model coefficients are $\alpha_{q,j,i,l}$, $\beta_{q,j,i,l}$, $\gamma_{q,j,i,l}$ and $\delta_{q,j,i,l}$. The Parallel Hammerstein model has been proven to have superior linearization performance as compared to the COMP Model but with an increased count of coefficients [9].

IV. MEASUREMENT SETUP

The measurement setup consists of an arbitrary waveform generator (AWG 5204), having four channels from Tektronix. The setup also consists of 14 dB designed couplers, ZX60-V63+ power amplifiers which has an operating frequency range from 0.05 to 6 GHz, attenuators, a designed

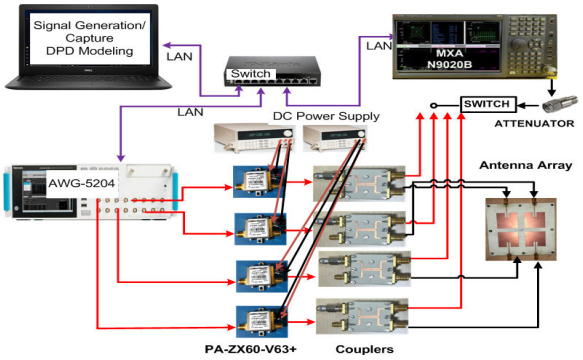

FIGURE 4. Block diagram of experimental setup.

antenna array, vector signal analyzer (VSA-MXAN9020B) from Keysight Technologies. The block diagram for the same is shown in Fig. 4. The antenna is made up of a rectangular four-element antenna array with microstrip patch elements. The highest coupling factor is around −20 dB between two array members. The S-parameters (S11, S12, S13 and S14) are shown in Fig. 5(a) for the frequency range from 3.3 GHz to 3.5 GHz. The S-parameter for coupler are shown in Fig. 5(b). The picture of antenna array and coupler are shown in Fig. 5(c) and Fig. 5(d). The signals are created in MATLAB and loaded in the AWG system, where it is transmitted and then captured using VSA. The central frequency used in the experiment is 3.45 GHz.

A. DEVICES AND SIGNALS UNDER TEST

A single data stream is split into four sub-data streams by spatial multiplexing MIMO precoding. Spatial multiplexing increases throughput by utilising the differences in channel characteristics between transmitting and receiving antenna pairs. It generates numerous independent streams between the transmitting and receiving antennas. The smaller number among the transmitting or receiving antennas is used to divide the channel into numerous streams in Singular Value Decomposition (SVD). SVD can provide two separate streams for 2×2 and four streams for 4×4 (four transmit antennas and four receive antennas), which could possibly quadruple the throughput. The streams of sub-symbols are then ciphered and delivered to the appropriate transmitter, which is a standard QAM unit. A modulator maps the information bits to 16 QAM symbols. For channel estimation (CE), more pilot symbols are included. The cyclic prefix is used as a guard interval in the signal sequence, which is then processed using the Inverse Fast Fourier transform (IFFT). The transmit antennas send out an LTE-OFDM modulated signal with pilot symbols. These symbols are later utilized to estimate the channel. The block diagram for MIMO-OFDM signal generation is shown in Fig. 6(a). The CCDF plot for all the signals generated to transmit through MIMO branches is shown in Fig. 6(b). The PAPR of the signals generated is approximately 10 dB. Four power amplifiers are used to transmit these signals simultaneously. The maximum coupling at the PA's

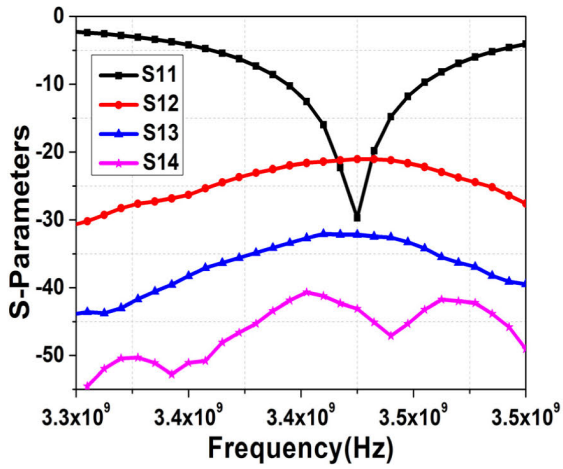

(a)

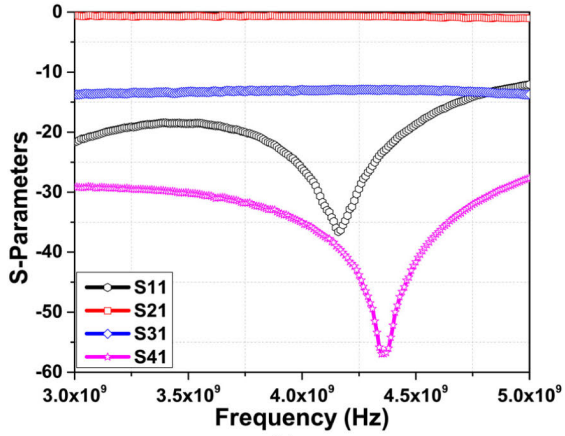

(b)

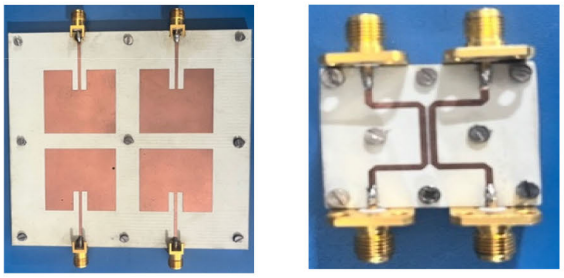

(c) (d)

FIGURE 5. (a) Measured antenna array S-parameters vs. frequency. The characteristics are only shown for antenna 1 since they are similar for all antennas due to reciprocity. (b) Coupler S-parameters vs. frequency. (c) Picture of antenna array (d) Picture of coupler.

output is achieved using -13dB couplers, with one output routed to the antenna and the other to the receiver. The factor between the two components of antennas is roughly -20dB. The other elements behave similarly because of the symmetry in the design of the antenna, as shown in Fig. 5. The four output signals from PA are measured with a Keysight MXA. The received signal has PA nonlinearity, cross-interference, and antenna reflection and is a linear combination of four transmitted signals.

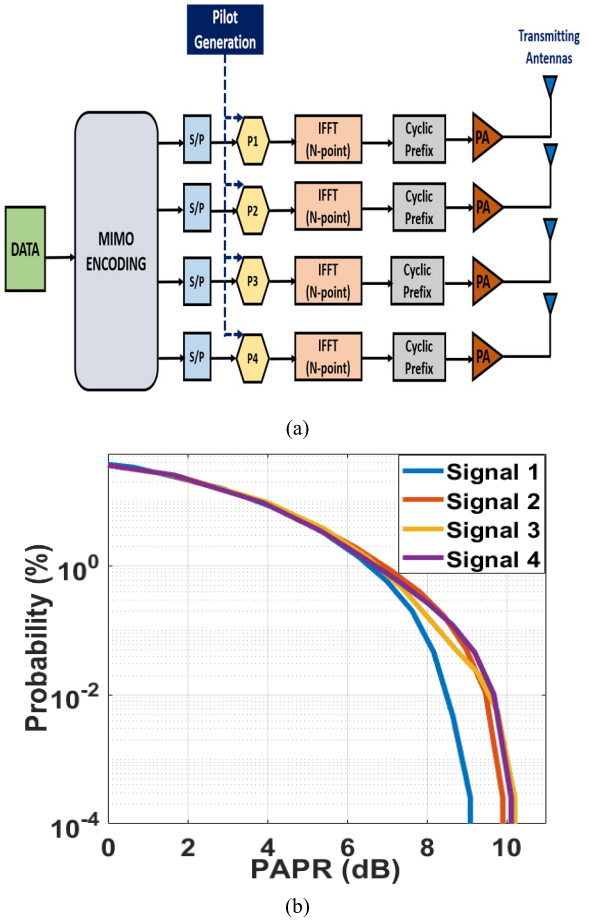

FIGURE 6. (a) Block diagram of MIMO-OFDM (b) CCDF plots of generated MIMO signals.

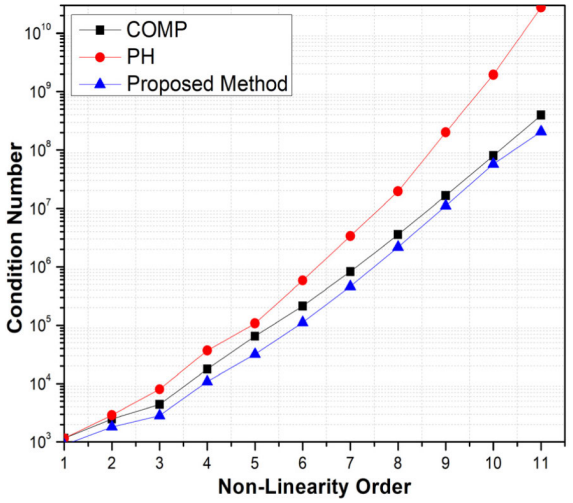

FIGURE 7. Condition number vs. Non-linearity order (M=5, Q=1 to 11).

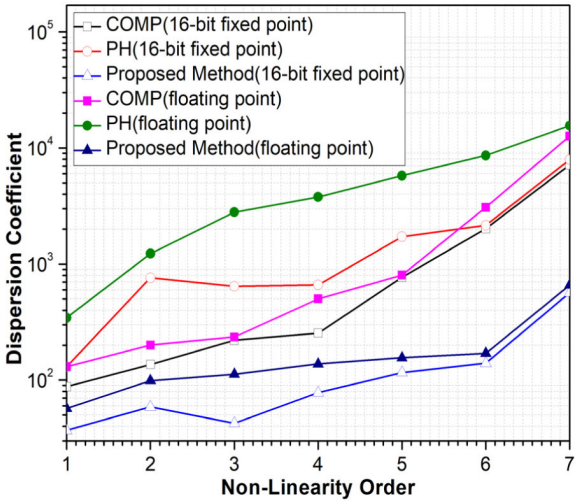

FIGURE 8. Dispersion coefficient for16-bit fixed-point arithmetic calculation and floating-point calculation for PH, COMP and proposed method (M=5, Q=1 to 8).

V. PERFORMANCE COMPARISON

The proposed DPD model was tested and compared to the pre-existing COMP Model, PH model, and without DPD. As mentioned in [21], Crosstalk in MIMO is due to different branches that lead to the mixing of signals. The proposed model finds an unmixing matrix A (described in section IIa) using Blind Source Separation (BSS). A better result was obtained with the application of the MP model with the aforementioned unmixing matrix. In the first scenario, we evaluate different results using the measurement equipment indicated in section IV and the signals/ PA described in IV-A and IV-B.

A. DPD MODEL PERFORMANCE METRICS

The NMSE computes in-band transmission error and is used to assess the DPD's performance [22]. It is calculated in decibels and is mathematically defined as:

$$NMSE_{dB} = 10 \times \log_{10}\left[\frac{\sum_{k=1}^{S} |y_{meas}(k) - x(k)|^2}{\sum_{k=1}^{S} |x(k)|^2}\right] \quad (24)$$

where, $x(k)$ is the complex baseband input signal, $y_{meas}(k)$ is the measured baseband output signal, and S denotes the total number of samples.

ACPR computes out-of-band transmission error [22] and may also be used to assess performance. It is evaluated as a ratio of adjacent channel power to main channel power in the frequency domain.

$$ACPR = \frac{1}{2}\left(\frac{\int_{f_c-\Delta f-\frac{BandWidth}{2}}^{f_c-\Delta f+\frac{BandWidth}{2}} |Y(f)|^2\,df + \int_{f_c+\Delta f-\frac{BandWidth}{2}}^{f_c+\Delta f+\frac{BandWidth}{2}} |Y(f)|^2\,df}{\int_{f_c-\frac{BandWidth}{2}}^{f_c+\frac{BandWidth}{2}} |Y(f)|^2\,df}\right) \quad (25)$$

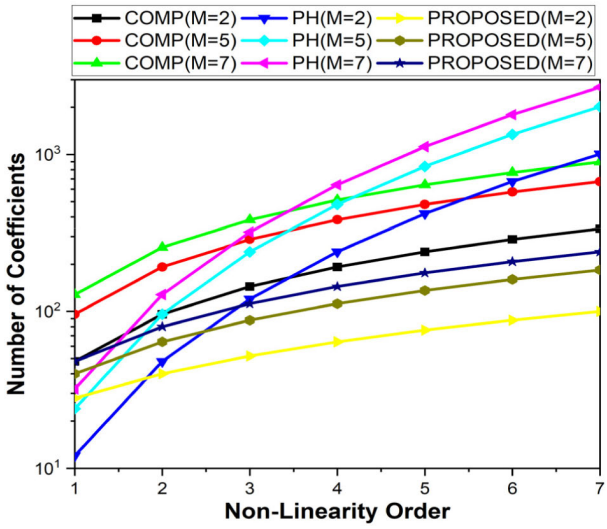

FIGURE 9. Number of coefficients vs non-linearity order (M=5, Q=1 to 7).

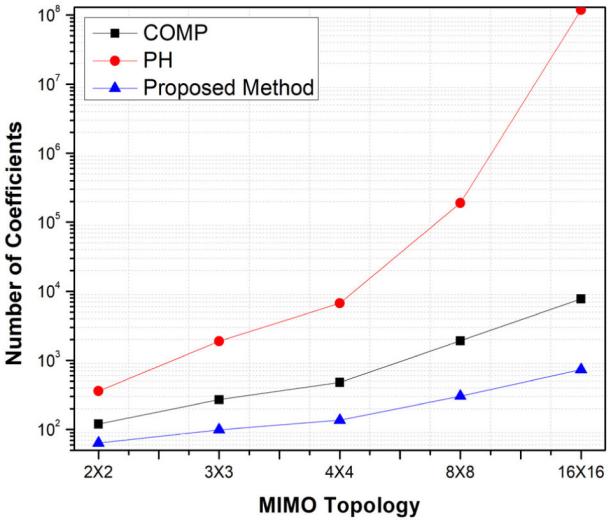

FIGURE 10. Number of coefficients vs MIMO topology (M=5, Q=5).

TABLE 1. Comparison of computational complexity and FPGA memory resources.

Method	PH	COMP	Proposed Method
Calculation of Coefficients for $T\times T$ MIMO	$T^2(M+1)Q(Q+1)(Q+2)/T!$	$T^2(M+1)Q$	$T(M+1)(Q)+T^2$
Number of Coefficients	840	480	136
Bit Resolution	16	16	16
Matrix Size	990904320	8257536	8257536
Memory Size (Megabytes) MB	1981.8	33.03	16.51

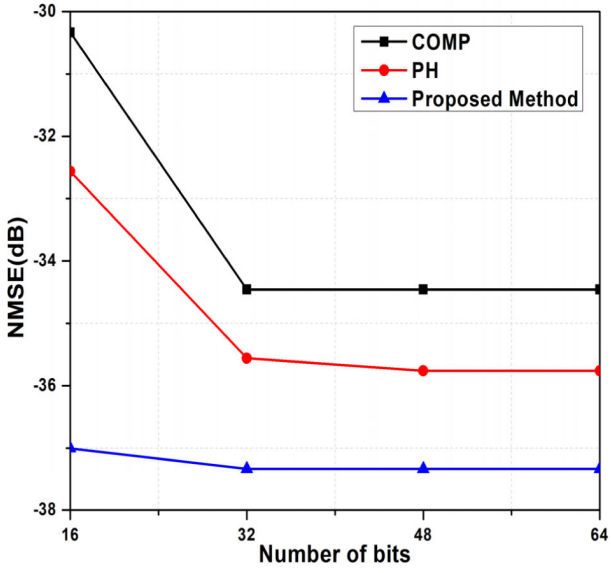

FIGURE 11. NMSE vs number of bits for M=5 and Q=5.

The modulation quality of the transmission can be computed using the EVM metric [23]. To calculate EVM, the received constellation is compared with the ideal constellation.

$$EVM = \sqrt{\frac{E\left\{\left|\hat{g}(k) - g(k)\right|^2\right\}}{E\left\{|g(k)|^2\right\}}} \tag{26}$$

where $g(k)$ and $\hat{g}(k)$ are the ideal symbol and measured symbol. E represents the expectation of ensemble averages.

B. NUMERICAL STABILITY

The statistic for determining a matrix's numerical stability is condition number. It calculates the propagation of error from the matrix to the Least Square solution [24]. The observation matrix's condition number is determined as follows:

$$\text{Condition number} = \frac{\lambda_{\max}}{\lambda_{\min}} \tag{27}$$

where λ_{max} and λ_{min} are the observation matrix's maximum and minimum singular values. The condition number of the observation matrix for different models, when the nonlinearity order varies from Q=1 to 11, is shown in Fig. 7. Lower condition number results in a better-conditioned and numerically stable matrix. In a fixed-point computation situation, the dispersion coefficient is also an important statistic for evaluating the success of the implementation. It depicts the number of bits which are required to cover the complete region of DSP coefficients with appropriate precision. It is expressed numerically as

$$\text{Dispersion Coefficient} = \frac{\max(|Coeff|)}{\min(|Coeff|)} \tag{28}$$

where Coeff denotes the value of coefficients. Fig. 8 shows the dispersion coefficient versus nonlinearity order in which

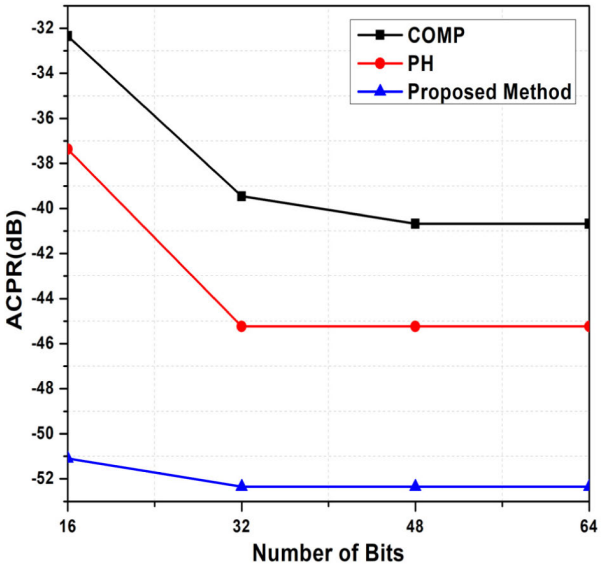

FIGURE 12. ACPR vs number of bits for M=5 and Q=5.

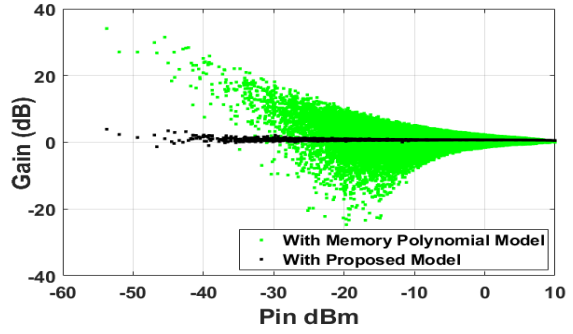

(a)

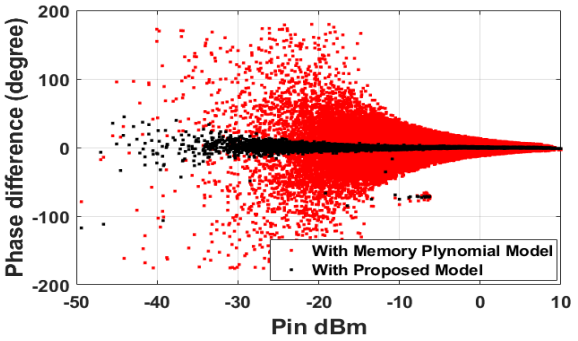

(b)

FIGURE 13. (a) AM/AM and (b) AM/PM graphs for memory polynomial and proposed model.

M=5, and the nonlinearity order varies from Q=1 to 7. Dispersion coefficients were analyzed for the 16-bit fixed point and floating-point calculations. Lower coefficient dispersion allows better precision while implementing DPD on a digital platform. When the coefficients are widely spread, the precision level of the coefficients in lower-bit fixed-point DSP is compromised. For instance, if the dispersion coefficient is 2n, at least two n-bits of resolution are needed

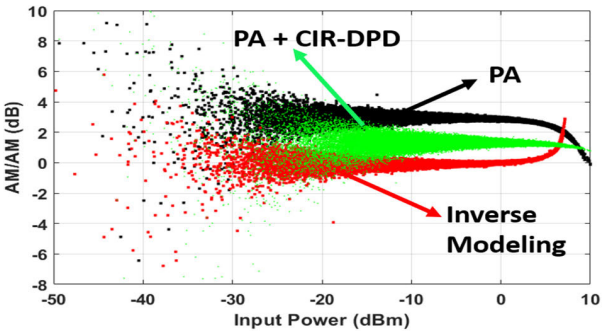

FIGURE 14. AM-AM plot for PA response, inverse modeling and PA with proposed CIR-DPD after cross-interference reduction.

TABLE 2. Comparison of linearization performance of DPD models.

Method	NMSE (dB)			
	Branch 1	Branch 2	Branch 3	Branch 4
No-DPD	-5.89	-6.67	-9.74	-7.67
COMP	-26.45	-27.35	-30.12	-28.87
PH	-29.55	30.778	-32.82	-30.09
Proposed Method	-31.78	-32.823	-35.476	-33.91
Method	ACPR (dB)			
	Branch 1	Branch 2	Branch 3	Branch 4
No-DPD	-31.91	-32.45	-32.55	-32.11
COMP	-44.56	-45.41	-47.34	-46.71
PH	-45.00	-47.23	-51.33	-49.23
Proposed Method	-51.33	-52.56	-54.04	-53.45

to maintain precision [25]. It is an important metric because coefficients in the Digital Predistortion method are stored in FPGA memory. The smaller coefficient dispersion suggests that coefficients can be stored with better precision and the proposed solution uses much less memory resources. It can be observed that the proposed model has the lowest dispersion coefficient as compared to other models in both fixed-point and floating-point calculations.

C. COMPUTATIONAL COMPLEXITY

Computational complexity is measured in terms of the number of coefficients in the DPD Model. It enhances with the increase in memory depth and nonlinearity order. Therefore, it becomes imperative to use the computationally efficient technique, which can work on low memory depth and nonlinearity order. Fig. 9 shows the comparison between the coefficients of all the models used in this study for the nonlinearity order varying from 1 to 7. $T(M+1)Q$ is the count of coefficients required by the COMP model for a single transmitter branch in $T\times T$MIMO [9]. As a result, the COMP model in $T\times T$MIMO requires a total of $T^2(M+1)Q$ coefficients [25]. $T(M+1)Q(Q+1)(Q+2)/T!$ is the coefficient count needed by the PH model for a single transmitter branch in

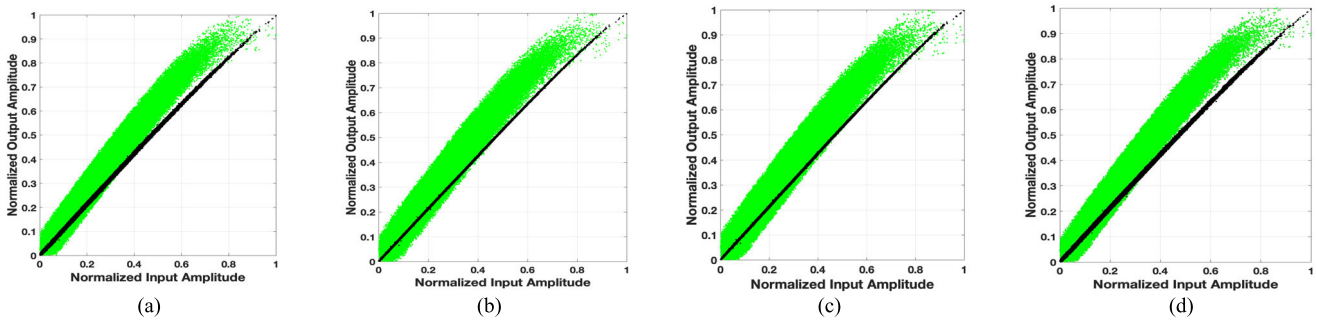

FIGURE 15. PA linearization in terms of normalized input vs. Output amplitude plots for (a) PA1 (b) PA2 (c) PA3 (d) PA4.

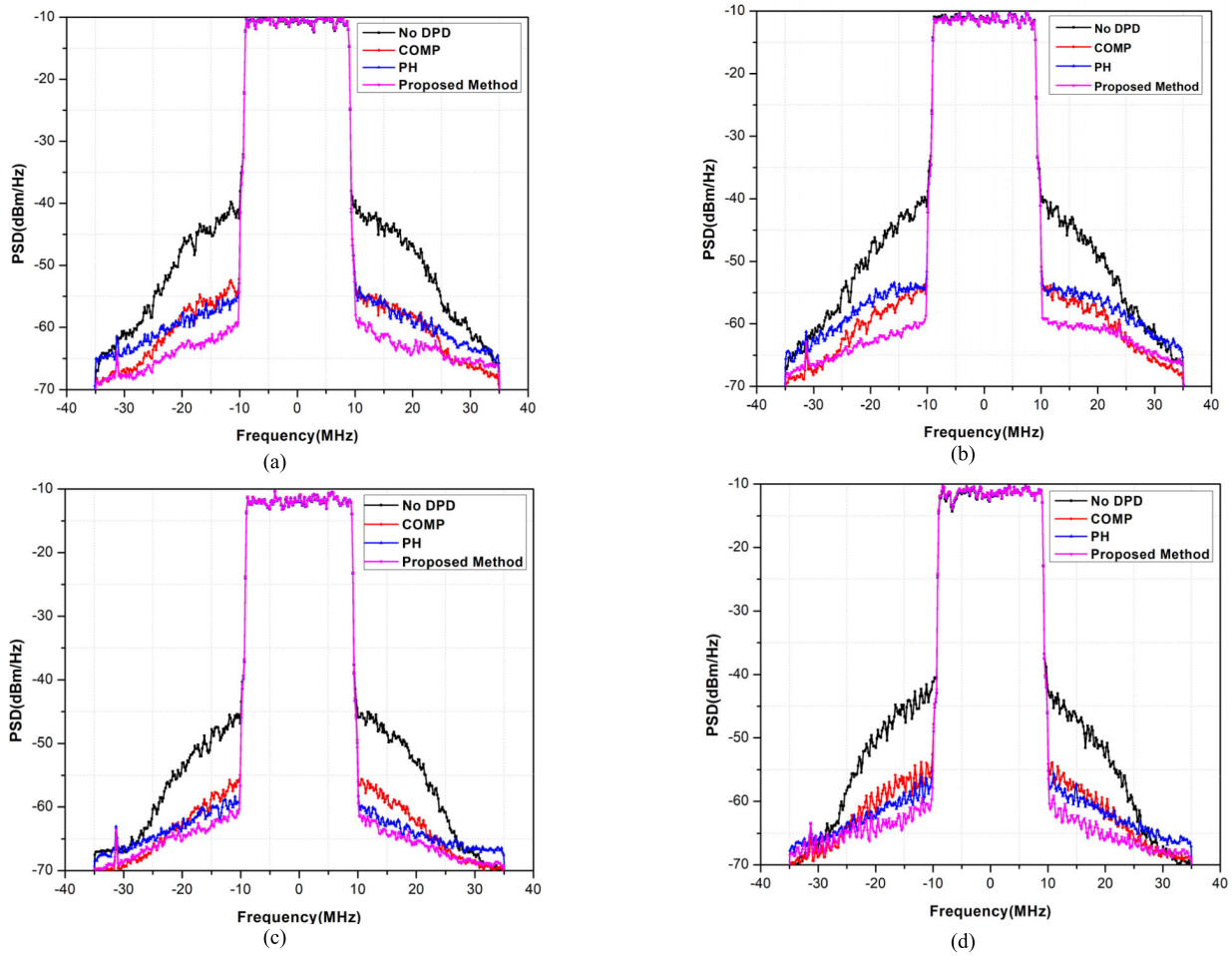

FIGURE 16. Frequency power spectra at the Centre frequency of 3.45 GHz for various DPD models in four branch MIMO transmitter (a) Branch 1 (b) Branch 2 (c) Branch 3 (d) Branch 4.

$T \times T$MIMO [25], and $T^2(M+1)Q(Q+1)(Q+2)/T!$ is the total count of coefficients for all T branches. $T(M+1)(Q)+T^2$ is the total count of coefficients required in the CIR-DPD model for the $T \times T$ MIMO system. It shows that the suggested model gives the minimum count of coefficients. This is due to the prior anticipation of crosstalk and antenna reflection coefficients obtained from Independent Component Analysis. Further, for higher MIMO topology or the Massive MIMO, the complexity grows with the increment in the number of branches. As the number of branches increases, the number of coefficients drastically surges. Fig. 10 shows the number of coefficients for PH, COMP, and the Proposed CIR-DPD model varying with 2×2, 3×3, 4×4, 8×8, and 16×16 MIMO topology. The results are calculated for higher topologies through simulation. Among all the models, CIR-DPD has the smallest number of coefficients.

TABLE 3. Table of comparison.

Work	Method	ACPR (dB)	NMSE Improvement(dB)	Number of Coefficients	Condition Number	Algorithm	Non-linearity Order(Q), Memory Depth(M)
[12]	CTMM Coefficient identification and Dual-input DPD	-51.5	19.70	139	Not mentioned	Iterative	Not mentioned
[27]	LMS & RLS Method for adaptation of CTC-DPD	-4[5.7	24.12	144	5.46×10^{7}	100 Iterations	Q=9, M=3
[28]	Two compensation blocks, static DPD and dynamic DPD for each channel	-53.21	24.23	1580	7.42×10^{10}	15 Iterations	$Q1$=7, $M1$=10 $Q2$=7, $M2$=5
[29]	Dual Input S-parameter based DPD Model	-47.1	23.9	Model Coefficients + S-parameters	Not mentioned	Iterative	*Q1 = 9, Q2 = Q3 = 5, M1 = 2, M2 = M3 = M4 = M6 = 1, and M5 = 0,*
This work	CIR using ICA, Basic Memory Polynomial for DPD	-54.04	25.74	136	4.34×10^{4}	Non-Iterative	Q=5, M=5

D. EFFECTIVENESS OF FIXED-POINT IMPLEMENTATIONS

Bit resolution is crucial when utilizing the digital predistortion because of the exponential growth in the number of coefficients with increasing MIMO topologies. The FPGA must operate in a fixed-point environment in order to do the processing faster. The memory size determines the total number of LUTs required in FPGA [10]. A model's memory requirements are determined by the size of the observation matrix and bit resolution. Usually, the model extraction is done with floating-point calculation in a DSP processor. The extracted model should be implemented in FPGA for smooth operations [26]. Table 1 compares the FPGA's memory resource use for continuous ZX60-V63+ PA inverse modeling using the PH model, COMP model, and suggested CIR-DPD model with 16-bit fixed-point calculation (M =5 Q = 5 and Input Length, L = 199608). The proposed CIR-DPD model has the best linearization performance at 16 bits with the fewest coefficients of all models. It requires the least amount of memory and LUTs. Fig. 8 depicts the improvement in the dispersion coefficient with the 16-bit fixed-point calculation compared to the floating-point calculation. Fig.11 and Fig. 12 shows the modeling performance of COMP, PH, and the proposed model for the fixed-point word length of 16, 32, 48, and 64 bits. The performance of the model degrades noticeably when implemented in a 16-bit fixed-point. The proposed model, on the other hand, significantly outperforms the other models.

VI. RESULTS AND DISCUSSION

The efficacy of COMP, PH, and the proposed CIR-DPD models are evaluated through a 4 × 4 MIMO system. The proof-of-concept is carried out by AWG-5204 four-channel MIMO, and the four baseband signals are fed to the AWG system. All the signals are transmitted simultaneously through PA1, PA2, PA3, PA4 and then fed into a microstrip antenna. For convenience, all power amplifiers used are ZX60-V63+. The proposed method uses a two-step method. First, Cross-interference reduction, and then the application of Memory Polynomial DPD. Fig. 13 shows that without cross-interference reduction, the AM-AM and AM-PM plots after memory polynomial-based DPD come out scattered, whereas the AM-AM and AM-PM plots for the proposed method are clean. Fig.14 shows the AM-AM plots of the PA response, inverse modeling performed with the Proposed CIR-DPD Model, and PA with the Proposed CIR- DPD response. All three responses are plotted after the cross-interference reduction. Table 2 compares the linearization performance in terms of ACPR and NMSE of PH, COMP, and the CIR-DPD Model proposed in this study. The average output power of the PAs is 6 dBm, and -2 dBm OPBO has been applied at which the ACPR and NMSE were obtained. The proposed method gives the best results with low computational complexity. Fig. 15 (a), (b), (c), and (d) shows the input vs. output voltage plot for PA and PA with the CIR-DPD model for all four branches of the MIMO transmitter. Fig. 16 (a), (b), (c), and (d) displays the frequency spectra of several models for all four branches of the 4 × 4 MIMO system used for proof-of-concept. Compared to conventional MIMO-DPD, [12] uses the dual-input memory polynomial PA model to identify the crosstalk and mismatch (CTMM) coefficients. It is a two-step procedure. The dual-input PA model's coefficients are first estimated. The CTMM coefficients are then computed using the obtained PA model coefficients. The two steps of the technique are conducted iteratively until the desired outcome

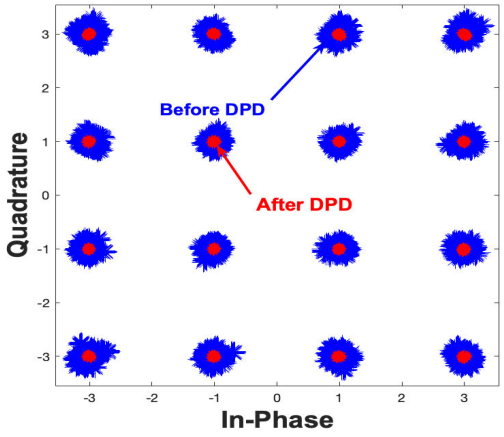

FIGURE 17. Constellation diagrams for before and after DPD.

TABLE 4. Comparison of EVM for different DPD models.

MODEL	EVM (dB)
No DPD	-22.1932
COMP	-39.4938
PH	-39.8279
Proposed Model	-41.1103

is achieved. After that, the dual-input DPD is applied for PA nonlinearity. Time complexity and coefficient adaptation complexity are always high in an iterative method. In [27], the linearization is done by adaptive Recursive Least Squares (RLS) and Least Mean Squares (LMS), where the DPD and crosstalk coefficients are updated for every sample. The complexity of this method rises as the number of transmit paths grows because the inversion of the crosstalk matrix for CTC-DPD requires great computational effort. As the number of filter coefficients that models the crosstalk increases, the complexity of the CTC-DPD method also rises. In [28], a MIMO interference cancellation based on a CTC-DPD was used to remove nonlinear crosstalk components. A complex memoryless polynomial model and a complex GMP model were used to capture static and dynamic effects, which was made possible by a cascaded DPD architecture. Table 3 presents a comprehensive experimental comparison of select state-of-the-art linearization approaches. This evaluation is conducted under identical experimental conditions as the proposed method. The proposed method is a two-step procedure in which cross-interference reduction is followed by the DPD method with a single iteration, in contrast to [27] and [28], which are iterative and initial conditions for convergence are to be investigated. It is faster than other DPD methods used in [27] and [28] because it requires a single run.

Fig. 19(a) shows the variation NMSE and ACPR versus the nonlinearity order for different MIMO waveforms of 10 MHz, 20 MHz, and 50 MHz. These waveforms have varying characteristics, such as different PAPRs shown in

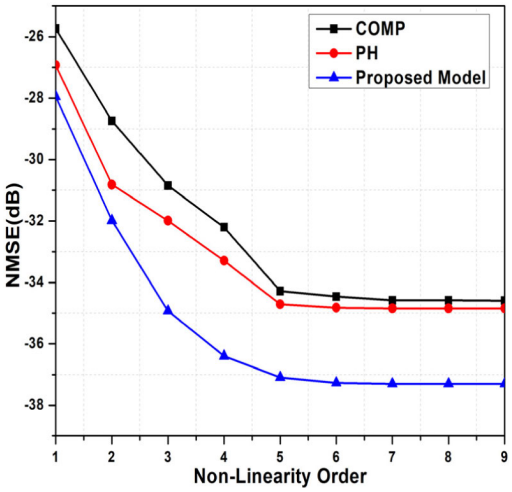

FIGURE 18. NMSE vs non-linearity order for M=5.

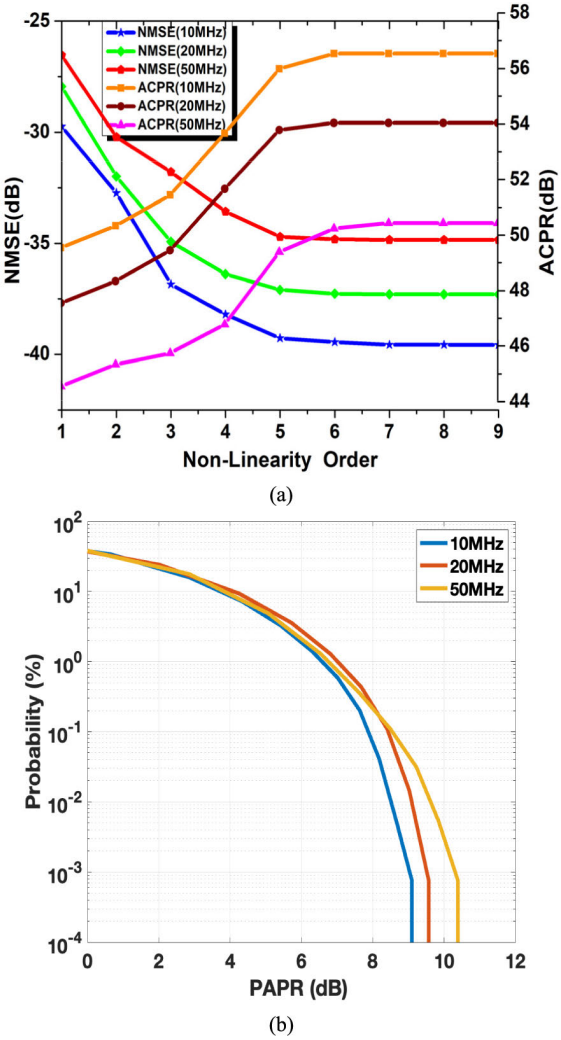

FIGURE 19. (a) Plots of NMSE, ACPR vs non-linearity order for different signals (b) PAPR of different signals.

Fig. 19(b) and mean power levels. The plots demonstrate that our proposed method exhibits consistent performance

across other signals, irrespective of their characteristics, highlighting the robustness of the proposed method. This method can be utilized at base stations to linearize the PA and remove cross-interference for MIMO systems. After performing DPD, the EVM is calculated, shown in Table 4. Fig. 17 shows the constellation diagram for the data when no DPD is applied compared to the Proposed CIR-DPD model. Fig. 18 shows the NMSE performance for nonlinearity order from 1 to 9 and a memory depth 5. It implies that the suggested model improves linearization performance and computational complexity for lower {Q, M}. Due to spatial multiplexing precoding, all the MIMO signals areuncorrelated, allowing ICA to function effectively. In contrast, ICA cannot be used in beamforming because the signals at each PA become strongly correlated. In this scenario, it is advisable first to determine the crosstalk pre-cancellation coefficients using uncorrelated signals. Further, apply DPD on correlated signals for beamforming using the initially identified crosstalk pre-cancellation coefficients.

VII. CONCLUSION

This paper presents a computationally efficient linearization method and crosstalk reduction in MIMO topology. The proposed Cross-Interference Reduction Digital Predistortion (CIR-DPD) model is implemented in 4×4 MIMO transmitters having defects such as crosstalk, PA nonlinearity, and antenna reflection. The proposed method uses independent component analysis to model the crosstalk and inverse crosstalk coefficients while modeling the predistorted signal. Compared to other DPD models, the CIR-DPD model produces good performance with fewer coefficients as the number of MIMO transmitters grows. Compared to other conventional DPD models, the computational efficiency of the dispersion coefficient and condition number is also promising. Hence, the memory resource utilization for the CIR-DPD model reduces significantly. This proposed approach might be used to linearize large MIMO for 5G wireless communication while compensating for additional distortions.

REFERENCES

[1] E. G. Larsson, O. Edfors, F. Tufvesson, and T. L. Marzetta, "Massive MIMO for next generation wireless systems," *IEEE Commun. Mag.*, vol. 52, no. 2, pp. 186–195, Feb. 2014.

[2] Q. H. Spencer, A. L. Swindlehurst, and M. Haardt, "Zero-forcing methods for downlink spatial multiplexing in multiuser MIMO channels," *IEEE Trans. Signal Process.*, vol. 52, no. 2, pp. 461–471, Feb. 2004.

[3] L. Guan and A. Zhu, "Green communications: Digital predistortion for wideband RF power amplifiers," *IEEE Microw. Mag.*, vol. 15, no. 7, pp. 84–99, Nov. 2014.

[4] F. M. Ghannouchi and O. Hammi, "Behavioral modeling and predistortion," *IEEE Microw. Mag.*, vol. 10, no. 7, pp. 52–64, Dec. 2009.

[5] J. Wood, *Behavioral Modeling and Linearization of RF Power Amplifiers*. Norwood, MA, USA: Artech House, 2014.

[6] P. P. Campo, A. Brihuega, L. Anttila, M. Turunen, D. Korpi, M. Allén, and M. Valkama, "Gradient-adaptive spline-interpolated LUT methods for low-complexity digital predistortion," *IEEE Trans. Circuits Syst. I, Reg. Papers*, vol. 68, no. 1, pp. 336–349, Jan. 2021.

[7] C.-F. Cheang, P.-I. Mak, and R. P. Martins, "A hardware-efficient feedback polynomial topology for DPD linearization of power amplifiers: Theory and FPGA validation," *IEEE Trans. Circuits Syst. I, Reg. Papers*, vol. 65, no. 9, pp. 2889–2902, Sep. 2018.

[8] S. A. Bassam, M. Helaoui, and F. M. Ghannouchi, "Crossover digital predistorter for the compensation of crosstalk and nonlinearity in MIMO transmitters," *IEEE Trans. Microw. Theory Techn.*, vol. 57, no. 5, pp. 1119–1128, May 2009.

[9] A. Abdelhafiz, L. Behjat, F. M. Ghannouchi, M. Helaoui, and O. Hammi, "A high-performance complexity reduced behavioral model and digital predistorter for MIMO systems with crosstalk," *IEEE Trans. Commun.*, vol. 64, no. 5, pp. 1996–2004, May 2016.

[10] P. Jaraut, M. Rawat, and F. M. Ghannouchi, "Composite neural network digital predistortion model for joint mitigation of crosstalk, I/Q imbalance, nonlinearity in MIMO transmitters," *IEEE Trans. Microw. Theory Techn.*, vol. 66, no. 11, pp. 5011–5020, Nov. 2018.

[11] Z. A. Khan, E. Zenteno, P. Händel, and M. Isaksson, "Digital predistortion for joint mitigation of I/Q imbalance and MIMO power amplifier distortion," *IEEE Trans. Microw. Theory Techn.*, vol. 65, no. 1, pp. 322–333, Jan. 2017.

[12] K. Hausmair, P. N. Landin, U. Gustavsson, C. Fager, and T. Eriksson, "Digital predistortion for multi-antenna transmitters affected by antenna crosstalk," *IEEE Trans. Microw. Theory Techn.*, vol. 66, no. 3, pp. 1524–1535, Mar. 2018.

[13] A. T. Erdogan, "A simple geometric blind source separation method for bounded magnitude sources," *IEEE Trans. Signal Process.*, vol. 54, no. 2, pp. 438–449, Feb. 2006.

[14] A. Hyvärinen and E. Oja, "Independent component analysis: Algorithms and applications," *Neural Netw.*, vol. 13, nos. 4–5, pp. 411–430, Jun. 2000.

[15] W. L. Woo and S. S. Dlay, "Neural network approach to blind signal separation of mono-nonlinearly mixed sources," *IEEE Trans. Circuits Syst. I, Reg. Papers*, vol. 52, no. 6, pp. 1236–1247, Jun. 2005.

[16] P. Jaraut, G. C. Tripathi, M. Rawat, and P. Roblin, "Independent component analysis for multi-carrier transmission for 4G/5G power amplifiers," in *Proc. 89th ARFTG Microw. Meas. Conf. (ARFTG)*, Honolulu, HI, USA, Jun. 2017, pp. 1–4.

[17] A. Hyvarinen, "Fast and robust fixed-point algorithms for independent component analysis," *IEEE Trans. Neural Netw.*, vol. 10, no. 3, pp. 626–634, May 1999.

[18] X. Yu and H. Jiang, "Digital predistortion using adaptive basis functions," *IEEE Trans. Circuits Syst. I, Reg. Papers*, vol. 60, no. 12, pp. 3317–3327, Dec. 2013.

[19] Y.-S. Chen and C.-A. Lin, "Blind-channel identification for MIMO single-carrier zero-padding block-transmission systems," *IEEE Trans. Circuits Syst. I, Reg. Papers*, vol. 55, no. 6, pp. 1571–1579, Jul. 2008.

[20] S. Coleri, M. Ergen, A. Puri, and A. Bahai, "Channel estimation techniques based on pilot arrangement in OFDM systems," *IEEE Trans. Broadcast.*, vol. 48, no. 3, pp. 223–229, Sep. 2002.

[21] S. Amin, P. N. Landin, P. Händel, and D. Rönnow, "Behavioral modeling and linearization of crosstalk and memory effects in RF MIMO transmitters," *IEEE Trans. Microw. Theory Techn.*, vol. 62, no. 4, pp. 810–823, Apr. 2014.

[22] P. Landin, M. Isaksson, and P. Handel, "Comparison of evaluation criteria for power amplifier behavioral modeling," in *IEEE MTT-S Int. Microw. Symp. Dig.*, Jun. 2008, pp. 1441–1444.

[23] A. Mohammadi and F. M. Ghannouchi, *RF Transceiver Design for MIMO Wireless Communications*, vol. 145. Cham, Switzerland: Springer, 2012.

[24] A. H. Abdelhafiz, A. Zerguine, O. Hammi, and F. M. Ghannouchi, "Lattice-based memory polynomial predistorter for wideband radio frequency power amplifiers," *IET Commun.*, vol. 8, no. 17, pp. 3122–3127, Nov. 2014.

[25] E. W. Cheney and D. R. Kincaid, *Numerical Mathematics and Computing*, 7th ed. Pacific Grove, CA, USA: Brooks/Cole, 2008.

[26] M. V. Amiri, S. A. Bassam, M. Helaoui, and F. M. Ghannouchi, "Estimation of crossover DPD using orthogonal polynomials in fixed point arithmetic," *AEU Int. J. Electron. Commun.*, vol. 67, no. 11, pp. 905–909, Nov. 2013.

[27] P. M. Suryasarman and A. Springer, "A comparative analysis of adaptive digital predistortion algorithms for multiple antenna transmitters," *IEEE Trans. Circuits Syst. I, Reg. Papers*, vol. 62, no. 5, pp. 1412–1420, May 2015.

[28] T. Ackermann, J. Potschka, T. Maiwald, A. Hagelauer, G. Fischer, and R. Weigel, "A robust digital predistortion algorithm for 5G MIMO: Modeling a MIMO scenario with two nonlinear MIMO transmitters including a cross-coupling effect," *IEEE Microw. Mag.*, vol. 21, no. 7, pp. 54–62, Jul. 2020.

[29] K. Hausmair, S. Gustafsson, C. Sánchez-Pérez, P. N. Landin, U. Gustavsson, T. Eriksson, and C. Fager, "Prediction of nonlinear distortion in wideband active antenna arrays," *IEEE Trans. Microw. Theory Techn.*, vol. 65, no. 11, pp. 4550–4563, Nov. 2017.

SHIPRA (Student Member, IEEE) received the B.Tech. degree in electronics and communication engineering from AKTU, India, in 2015, and the M.Tech. degree in VLSI design from Indira Gandhi Delhi Technical University, New Delhi, India, in 2017. She is currently pursuing the Ph.D. degree in electronics and communication with the Indian Institute of Technology Roorkee, India. Her research interests include OTA MIMO communication, self-interference cancellation, and MIMO digital predistortion.

MEENAKSHI RAWAT (Member, IEEE) received the M.Sc. and Ph.D. degrees in electrical and computer engineering from the University of Calgary, Calgary, AB, Canada, in 2012. She was a Postdoctoral Research Fellow with the University of Calgary, from September 2012 to June 2013. She was also with Ohio State University as a Postdoctoral Project Researcher/Scientist, from July 2013 to June 2014. She is currently an Associate Professor with the Indian Institute of Technology (IIT) Roorkee, Uttarakhand. She is one of the founding directors of the IITR-led startup "Linearized amplifier technologies and services private ltd." She is also the CNSP Group Coordinator and a Coordinator with the Jio 5G Laboratory, IITR. She has developed several single-band, multiband, and ultra-wideband solutions to facilitate distortion-free front-end for five industrial projects, leading to three patents and over 95 IEEE TRANSACTIONS and conferences. She received the University of Calgary's Research Production Award three times and the Best Paper Award at the 82nd and 83rd ARFTG Conferences, in 2013 and 2014. She also receives the Young Faculty Research Fellowship from the Digital India Laboratories.